Journal of Biomedical Optics

BiomedicalOptics.SPIEDigitalLibrary.org

Development of Raman spectral markers to assess metastatic bone in breast cancer

Hao Ding
Jeffry S. Nyman
Julie A. Sterling
Daniel S. Perrien
Anita Mahadevan-Jansen
Xiaohong Bi

SPIE.

Development of Raman spectral markers to assess metastatic bone in breast cancer

Hao Ding,[a] Jeffry S. Nyman,[b,c,d,e] Julie A. Sterling,[b,e,f,g] Daniel S. Perrien,[b,d,e,h] Anita Mahadevan-Jansen,[c] and Xiaohong Bi[a,*]

[a]University of Texas Health Science Center at Houston, Department of Nanomedicine and Biomedical Engineering, 1881 East Road, Houston, Texas 77054
[b]Tennessee Valley Healthcare System, Department of Veterans Affairs, 1310 24th Avenue South, Nashville, Tennessee 37212
[c]Vanderbilt University, Department of Biomedical Engineering, VU Station B#351631, 2301 Vanderbilt Place, Nashville, Tennessee 37235
[d]Vanderbilt University, Department of Orthopaedic Surgery and Rehabilitation, Medical Center East, South Tower, Suite 4200, Nashville, Tennessee 37232
[e]Vanderbilt University, Vanderbilt Center for Bone Biology, 2215B Garland Avenue, Nashville, Tennessee 37232
[f]Vanderbilt University, Department of Medicine, Division of Clinical Pharmacology, 2200 Pierce Ave., Nashville, Tennessee 37235
[g]Vanderbilt University, Department of Cancer Biology, 2220 Pierce Ave., Nashville, Tennessee 37235
[h]Vanderbilt University, Institute of Imaging Sciences, 1161 21st Avenue South, Medical Center North, AA-1105, Nashville, Tennessee 37232

Abstract. Bone is the most common site for breast cancer metastases. One of the major complications of bone metastasis is pathological bone fracture caused by chronic bone loss and degeneration. Current guidelines for the prediction of pathological fracture mainly rely on radiographs or computed tomography, which are limited in their ability to predict fracture risk. The present study explored the feasibility of using Raman spectroscopy to estimate pathological fracture risk by characterizing the alterations in the compositional properties of metastatic bones. Tibiae with evident bone destruction were investigated using Raman spectroscopy. The carbonation level calculated by the ratio of carbonate/phosphate $\nu 1$ significantly increased in the tumor-bearing bone at all the sampling regions at the proximal metaphysis and diaphysis, while tumor-induced elevation in mineralization and crystallinity was more pronounced in the metaphysis. Furthermore, the increased carbonation level is positively correlated to bone lesion size, indicating that this parameter could serve as a unique spectral marker for tumor progression and bone loss. With the promising advances in the development of spatially offset Raman spectroscopy for deep tissue measurement, this spectral marker can potentially be used for future noninvasive evaluation of metastatic bone and prediction of pathological fracture risk. [DOI: 10.1117/1.JBO.19.11.111606]

Keywords: Raman spectroscopy; bone quality; bone composition; breast cancer; bone metastasis.

Paper 140115SSRR received Feb. 26, 2014; revised manuscript received May 17, 2014; accepted for publication May 20, 2014; published online Jun. 16, 2014.

1 Introduction

Breast cancer (BCa) is the second leading cause of cancer death in women in the United States, with >230,000 invasive BCa diagnoses and 40,000 deaths estimated in 2014.[1] Despite recent advances in health awareness, patient screening, and cancer treatment, a significant proportion of women still develop advanced BCa, among which ~70% will develop bone metastases, causing chronic bone loss and destruction.[2–4] As a result, pathological bone fractures occur and represent one of the most serious problems associated with metastasis.[5–7] Therefore, it is important to predict patients' fracture risk, thus providing guidance for personalized therapy. Current guidelines for the prediction of pathological fracture rely primarily on radiographs or computed tomography (CT). However, previous studies suggested that information from these examinations alone does not fully explain fracture risk.[8,9] Combining these current standards with other techniques could offer new opportunities to obtain complimentary information about bone quality and, therefore, improve the prediction of the risk for pathological fracture.

Raman spectroscopy (RS) is a vibrational spectroscopy technique that detects the inelastic scattering of photons upon their interactions with molecules. It provides molecular specific information regarding tissue's compositional properties, which are key determinants for bone quality. In the past decades, RS has been successfully applied to characterize alterations in bone composition caused by aging and disease.[10–13] McCreadie et al. studied women proximal femurs and suggested bone compositions as risk factors for osteoporotic fracture.[10] In another study, RS-derived bone material properties have exhibited significant correlation with the tissue-level mechanical function of bone, demonstrating promising potential in fracture risk prediction.[14]

Despite the promising results of RS in bone quality evaluation, the *in vivo* application of RS for orthopedic research has been limited by the shallow detection depth in the past decades. Both incident and Raman photons are highly scattered in biological tissues, hindering the technique's ability to detect deeper layers in turbid media. Recent advances in spatially offset Raman spectroscopy (SORS) permitted the detection of Raman signals from depth up to several millimeters and, in some cases, a couple of centimeters by introducing a distance between the illumination and collection fibers.[15–18] Schulmerich et al. demonstrated the measurement of bone Raman spectra

*Address all correspondence to: Xiaohong Bi, E-mail: Xiaohong.bi@uth.tmc.edu

from live mice with optimized fiber configuration.[15] Matousek et al. also successfully demonstrated that, using SORS, the spectrum of thumb distal phalanx could be obtained *in vivo* with a laser power below skin-safety level.[18] Such a breakthrough in penetration depth has opened the door for noninvasive *in vivo* Raman interrogation of bone constituents. Furthermore, based on the concepts of spatial offsetting and multichannel collection, Raman tomography (RT) of tissue phantoms has recently been developed, indicating the potential to obtain three-dimensional compositional mapping of bone tissue.[19,20]

Motivated by the need to improve fracture risk assessment in tumor-bearing bone and the promising advancement in SORS and RT, this study tries to determine the feasibility of assessing metastatic bone using RS. Tumor-bearing bones were investigated using Raman microspectroscopy to evaluate whether breast cancer metastases resulted in RS detectable local changes in bone tissue composition that may be linked to bone quality and fracture risk. The goal of the current study is to develop Raman spectral markers that are associated with tumor progression and resulting bone deterioration. These spectral markers may be used to evaluate the quality of metastatic bone and improve the estimation of the pathological fracture risk in the future in combination with noninvasive SORS and RT.

2 Methods

2.1 *Mouse Model for BCa Metastasis*

All animal studies were conducted in compliance with the National Institutes of Health guidelines as well as the Institutional Animal Care and Use Committee of Vanderbilt University and the University of Texas Health Science Center at Houston. MDA-MB-231 BCa cells (10^5 cells in 100 μl) were injected into the left ventricle of five-week-old female nude mice (Foxn nu-/-; Harlan, $n = 15$). The control group received a phosphate buffered saline injection ($n = 7$). The injection procedure was performed under anesthesia using previously reported methods.[21] The mouse was placed on its back with the limbs taped down. A 28 g ½ gauge needle attached to a 300-μl insulin syringe loaded with BCa cells was injected directly into the chest midway between the sternal notch and the top of xiphoid process, slightly left (anatomical) of the sternum. Once a bright red pulse of blood starts pumping back into the syringe, BCa cells were injected into the left cardiac ventricle. After the injection was complete, the needle was pulled straight out and the animal was kept on a heating pad until it fully recovered from anesthesia.

All mice were sacrificed at four weeks post tumor-inoculation. The tumor-bearing and control tibiae were harvested and cleaned of excess soft tissues before being stored in 70% alcohol at 4°C.

2.2 *Digital Radiograph*

Digital plane radiographs of the mice were acquired *in vivo* weekly using an XR-60 digital radiography system (Faxitron, Tucson, Arizona). Both tumor-bearing and control mice were imaged with an exposure of 35 kVp for 8 s while lying in a prone position under anesthesia. All radiographs were evaluated for tumor burden in a blinded fashion. The number and area of osteolytic bone metastases were calculated using the software MetaMorph (Molecular Devices Inc., Sunnyvale, California).[22,23]

2.3 *μ-Computed Tomography*

μCT was used to determine the mineralization, cortical, and trabecular architecture of the osteolytic lesions in tumor-bearing tibiae. After being removed from alcohol and dried on paper tissue, the proximal ends of the tibiae were imaged cross-sectionally in the μCT40 scanner (Scanco Medical, Bruttisellen, Switzerland). The regions of interest included both metaphysis and mid-diaphysis, and were typically scanned with the following parameters: an isotropic voxel size of 12 μm, x-ray source at 70 kVp and 114 μA, 250 projections per 180 deg, and an integration time of 300 ms. For segmentation of the bone from the surrounding soft tissues, a threshold of 411 mg HA/ccm, Sigma 0.2, and Support of 1 was used. Bone tissue mineral density (TMD) was quantified from cortical mid-diaphysis via Scanco evaluation software. Trabecular bone volume fraction (BV/TV), trabecular number (Tb.N), and trabecular spacing (Tb.Sp) were calculated from the proximal metaphysis as previously described.[24]

2.4 *Raman Measurement and Analysis*

Raman spectra of the tibial cortical bone were collected using a confocal Raman microscope (Renishaw Invia, Gloucestershire, England), as described previously.[14,25] In brief, the intact tibiae were mounted on a microscope slide with a small amount of polymer clay to help position the proximal metaphysis surface leveled horizontally. All the samples were measured with the same orientation with respect to the incident light, minimizing possible variations in Raman peak intensities caused by instrument polarization. Thirty milliwatts of a 785-nm laser light was focused through a Leica 50 × /0.50 objective on the cortical surface of the tibiae. The scattered Raman signals were collected through the same objective and coupled to a spectrometer and CCD camera for data acquisition. The Raman signals were collected every 500 μm on the proximal end of the tibiae, starting from metaphysis and extending to mid-diaphysis [Fig. 5(e)]. Two Raman spectra were acquired for each location, and a total of five locations (10 spectra) were collected for each tibia.

Raman spectra were processed for baseline correction using a modified polynomial fitting method.[25,26] Peak height at the maximum intensity and peak width at half max of selected Raman bands were calculated using custom-written MATLAB® scripts. The bone spectral signatures used in this study include phosphate $\nu 1$ (960 cm^{-1}), carbonate (1070 cm^{-1}), proline (856 cm^{-1}), and amide I (1665 cm^{-1}). Bone compositional properties were investigated by calculating mineralization (phosphate $\nu 1$/amide 1 and phosphate $\nu 1$/proline), mineral crystallinity (the reciprocal of the peak width at half max of phosphate $\nu 1$), and carbonation (carbonate/phosphate $\nu 1$).

2.5 *Statistics*

The statistical significance of tumor-associated changes in μCT and Raman spectral parameters was evaluated by Student's *t*-tests using SigmaPlot 12 software (Systat Software, Chicago, Illinois). The significance level was set at $p < 0.05$. The coefficient of variation (COV) was calculated by taking the ratio of the standard deviation to the mean of each Raman parameter from the control or tumor groups.

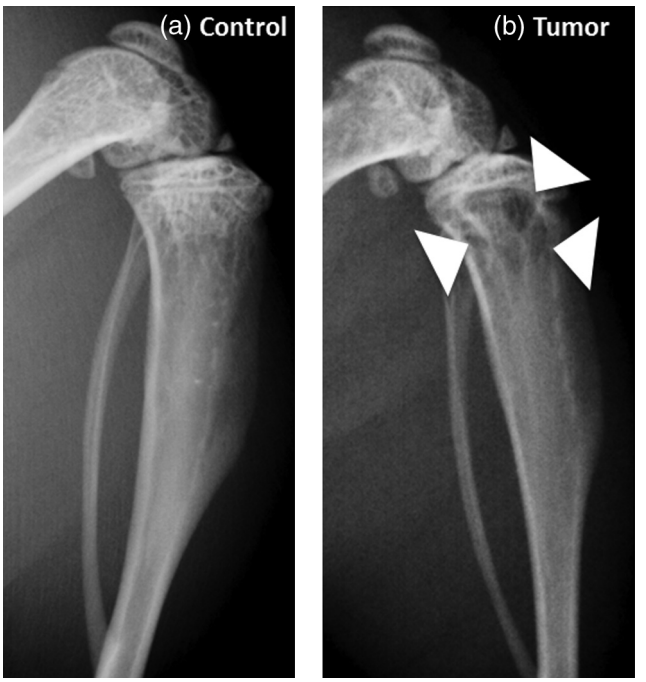

Fig. 1 Representative radiographs from the control (a) and the metastatic tibia (b). Osteolytic bone lesions are indicated by the white arrows.

3 Results

3.1 *Bone Structural and Architectural Changes Induced by BCa Metastasis*

BCa has been known to metastasize into bones and cause bone loss (osteolysis).[2,3,7] Representative radiographs in Fig. 1 exhibit the images from the control and the tumor-bearing tibiae. Most of the osteolytic lesions (indicated by white arrows) are in the metaphysis region. Further inspection of these lesions by μCT indicates that BCa metastases induced significant changes in the architectural properties of tibial metaphysis. A marked decrease in trabecular bone volume fraction and trabecular number [Figs. 2(a) and 2(b), both $p < 0.001$], and a significant increase in trabecular space [Fig. 2(c), $p < 0.001$] were observed in the metaphysis of tumor-bearing bone, confirming bone loss and structural disruption caused by BCa. No significant difference was observed in cortical TMD between tumor-bearing tibiae and the control group.

3.2 *RS Reveals Tumor-Associated Compositional Changes*

RS was used to measure mineral and matrix constituents of tibial cortical bones, with special interest at the metaphysis region where metastasis generally starts. Representative Raman spectra from tumor-bearing and control tibiae were compared in Fig. 3.

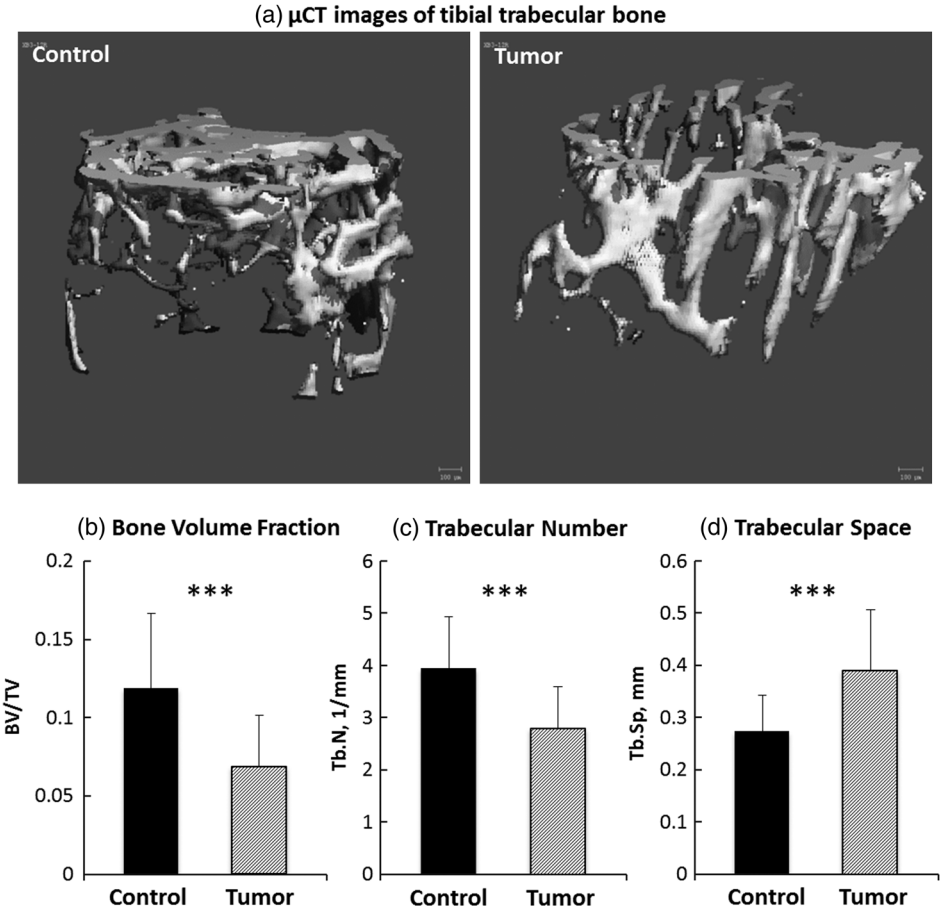

Fig. 2 μCT analysis of metastatic tibiae. Significant bone loss was observed in the trabecular bone of tumor-bearing tibia (a). Significantly reduced bone volume fraction (b), trabecular number (c), and enhanced trabecular space (d) indicate bone loss and architectural disruption in metastatic tibiae (***p<0.001).

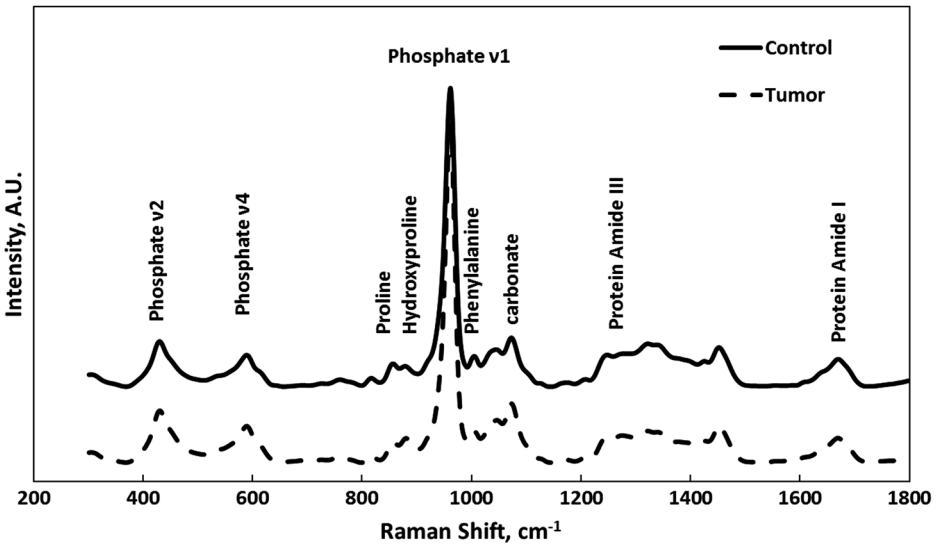

Fig. 3 Representative Raman spectra from tumor-bearing (dashed line) and control (solid line) tibiae. Selective Raman peaks are labeled on the figure.

Selective Raman peaks, including phosphate, proline, hydroxyproline, phenylalanine, carbonate, and protein amide, are labeled in Fig. 3 with their corresponding biochemical assignments. The variations in the intensities of these Raman signature bands reveal the changes in molecular content and organization induced by BCa metastasis.

Quantitative analysis of cortical composition was performed by calculating the intensity of Raman features that were associated with tissue-level bone material properties in previous reports.[14] These spectral features include the degree of collagen mineralization, which is calculated by the peak ratio of phosphate $\nu 1$ and amide 1 (or proline); type B carbonate substitution level, which is determined by the peak ratio of carbonate and phosphate $\nu 1$; and hydroxyapatite crystallinity, which is calculated as the reciprocal of full width half maximum of phosphate $\nu 1$ peak. Figure 4 shows the comparison of the aforementioned

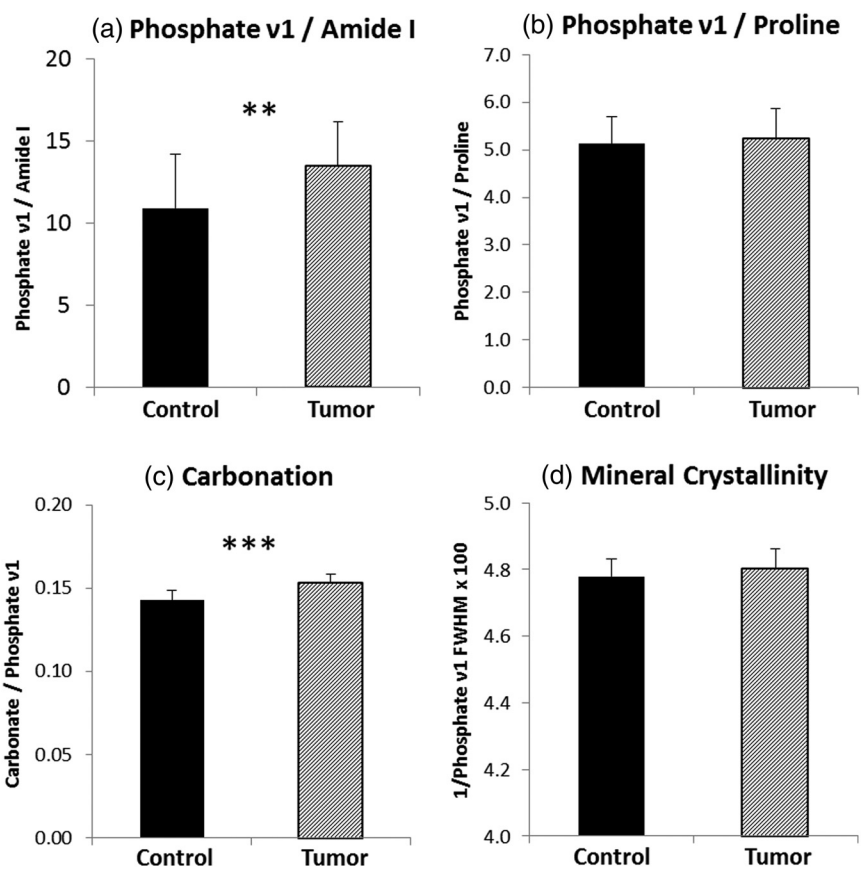

Fig. 4 Compositional parameters derived from Raman analysis. Significantly higher level of mineralization and carbonation was observed in tumor-bearing tibiae (*p<0.05; **p<0.01; ***p<0.001).

bone material properties between tumor-bearing and control tibiae when the averaged value from each bone was compared ($n = 30$ for tumor and $n = 14$ for control). The tumor-bearing group showed significant increases in mineralization (phosphate $\nu 1$/amide I) [Fig. 4(a)] and carbonate substitution [Fig. 4(c)], but no significant difference in mineral crystallinity [Fig. 4(d)] and phosphate $\nu 1$/proline [Fig. 4(b)].

To further evaluate the effect of tissue heterogeneity and proximity to tumor on the acquired spectral parameters, Raman spectra from the same relative location on tibiae were grouped and compared to four other sampling locations. Figure 5 shows tumor-associated compositional changes as a function of the distance to metaphysis. When sorted by locations, the elevation in mineralization is significant only at the proximal positions to metaphysis [Figs. 5(a) and 5(b)], where osteolytic lesions started and were most severe in all the animals (Fig. 1). Similarly, mineral crystallinity is significantly higher only at the metaphysis [Fig. 5(d)] in the tumor-bearing group. In contrast, carbonation level [Fig. 5(c)] was enhanced at all five measurement locations on the tibiae, indicating a possible alteration in bone material properties even in the absence of direct interaction with the tumor. Table 1 lists the COV in all the above compositional parameters from control and tumor groups. The variations in carbonation and mineral crystallinity are less pronounced than the mineralization parameters.

3.3 *Carbonation Level Is Correlated to the Size of Bone Lesions*

Pearson's correlation analysis was performed to interrogate the association between Raman-derived compositional properties and the size of bone lesions. The carbonation level showed significant positive correlation with the size of osteolytic lesions (Fig. 6), indicating that carbonate/phosphate $\nu 1$ could potentially be used as a spectral marker to evaluate tumor-induced bone degeneration.

4 Discussion

Bone is a common site for BCa metastasis.[27] In breast cancer patients, these bone metastases are typically osteolytic, or bone destructive.[2,3] Indeed, both digital radiograph and μCT results in our study showed osteolytic lesions in the tibiae of

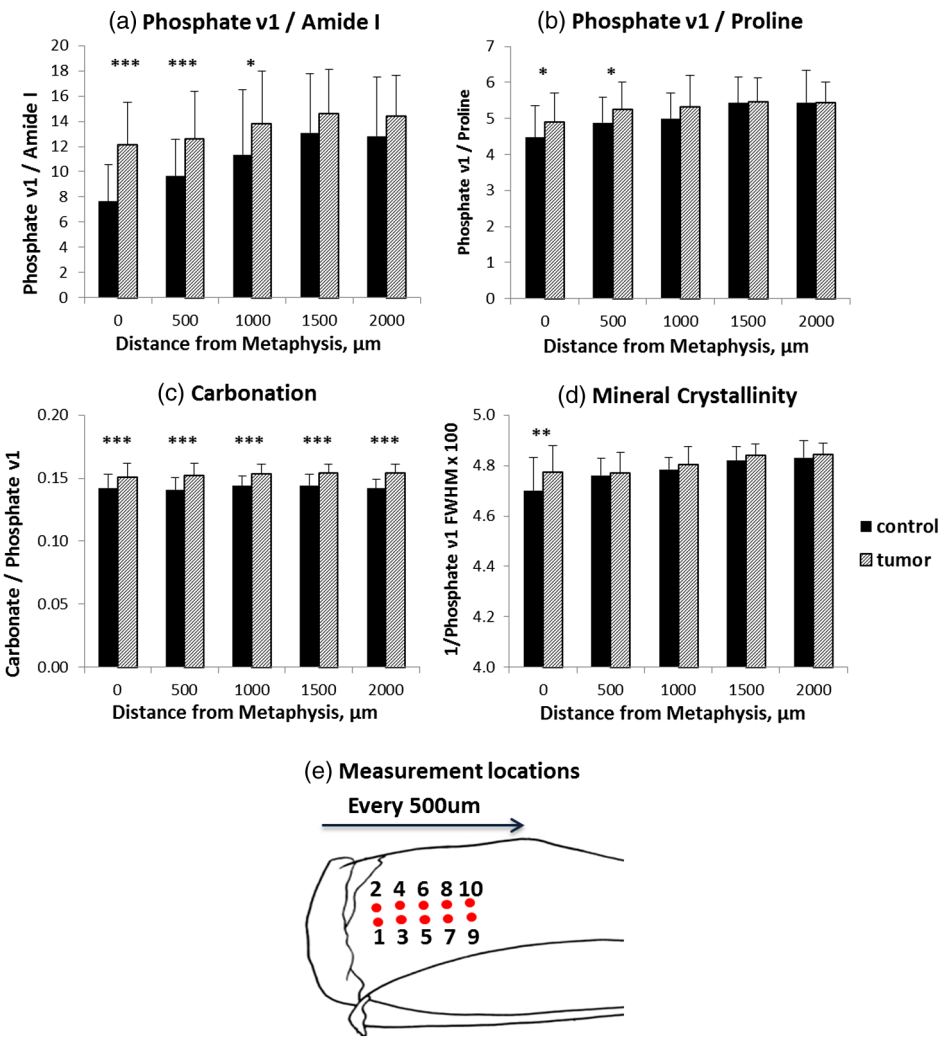

Fig. 5 Effect of tissue heterogeneity and proximity to tumor on Raman spectral parameters. Collagen mineralization by phosphate $\nu 1$/amide I (a) and phosphate $\nu 1$/proline (b), and mineral crystallinity (d) showed significant differences only at the proximal positions to metaphysis in the tumor-bearing tibiae, while carbonation level (c) was enhanced at all measurement locations. The measurement locations on tibiae are shown in (e). (*p<0.05; **p<0.01; ***p<0.001).

Table 1 The coefficient of variation in compositional parameters from control and tumor groups.

	Carbonation		Mineralization		Mineral/Collagen		Mineral crystallinity	
Measurement locations (μm)	Control (%)	Tumor (%)	Control (%)	Tumor (%)	Control (%)	Tumor (%)	Control (%)	Tumor (%)
0	7.56	6.58	36.22	23.86	19.96	16.37	2.68	1.60
500	6.86	6.65	26.15	26.41	14.48	14.43	1.42	1.10
1000	5.59	4.81	35.16	30.22	14.32	16.74	1.04	1.51
1500	6.70	4.60	36.59	23.98	13.39	11.99	1.22	0.98
2000	4.86	4.56	35.91	18.99	16.30	10.62	1.35	0.97

all tumor-bearing mice, which is in agreement with the bone structural changes observed in previous studies.[2–4]

While numerous studies have been focused on the structural and architectural changes of bone in BCa metastasis, other aspects of bone quality, particularly the compositional or material properties, have largely been neglected, likely due to a lack of effective detection methods. Bone TMD calculated from μCT has been suggested as an indicator for bone mineralization. However, μCT cannot detect the organic matrix in bone. Furthermore, the TMD value from the tumor-bearing tibiae in our study did not differ from that of the control group, indicating that μCT alone might not be enough to capture tumor-associated alterations in biochemical compositions. Therefore, techniques that can provide complementary information in bone composition can potentially expand current capability for bone quality evaluation. In the present study, the tumor-bearing tibiae exhibited significant differences in Raman-derived compositional properties, suggesting the feasibility to use RS for the detection of changes in bone quality related to breast cancer metastases.

Raman-derived compositional properties, including mineralization, mineral crystallinity, and carbonation, are important predictors of bone mechanical functions.[12,14,28] Studies on animal and human bones revealed that these Raman parameters are indicative of bone quality alterations associated with age and disease at tissue level.[29–31] Collagen mineralization indicates the amount of bone minerals, mainly consisting of calcium phosphate in an apatite crystalline structure, deposited in collagen matrix.[32,33] Hydroxyapatite crystallinity is an indicator for the size and stoichiometric perfection of the deposited mineral crystal.[34] Both properties have been found to increase with tissue age and demonstrated reduced heterogeneity within aged tissue, along with deteriorating mechanical properties.[12,29,31] Since bone is a birefringent material, the polarization of incident light and molecular orientation in the tissue can also affect the intensities of Raman bands.[35–38] The major vibration of phosphate $\nu1$ is along the direction of collagen fibrils, while the carbonyl groups (amide I) of collagen mainly stretch perpendicular to the fibrils. Therefore, both bands are very sensitive to sample orientation and the instrument polarization. The phase mismatch between phosphate $\nu1$ and amide I could introduce uncertainty when interpreting the difference of phosphate $\nu1$/amide I between groups. As a result, other Raman bands, such as phosphate $\nu2$ and $\nu4$, amide III, and proline, could be essential quality control parameters for compositional analysis.[35,37] The area ratio of phosphate $\nu2$ to amide III has been reported as insensitive to sample orientation, indicating phosphate $\nu2$/amide III is more relevant to the mineralization than phosphate $\nu1$/amide I.[36,37] Since the intensities of phosphate $\nu1$ and proline change with phase matching under polarized light, their ratio (phosphate $\nu1$/proline) has also been recommended for the calculation of mineralization.[35] In the current study, both phosphate $\nu1$/amide I and phosphate $\nu1$/proline have been investigated and demonstrated consistent outcomes at the metaphysis region (positions at 0 and 500 μm). The significance of differences (p value) between the two groups in phosphate $\nu1$/proline is not as dramatic as those in phosphate $\nu1$/amide I at the same position, indicating that there might be variations in the orientation of collagen fibrils besides mineralization in the tumor-bearing bones.

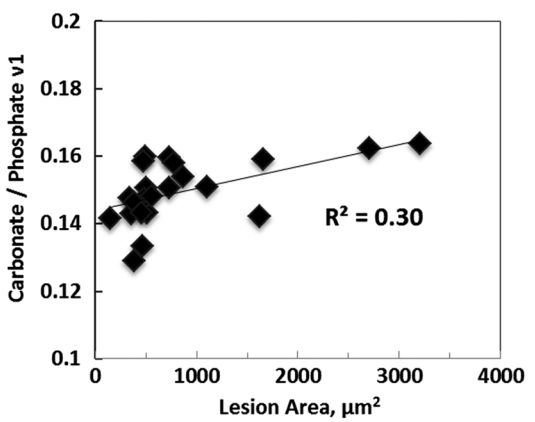

Fig. 6 Significant positive correlation was shown between carbonation level and the size of osteolytic lesions (p<0.05).

The development of bone metastases significantly alters the bone remodeling process and, thus causes pathologic compositional changes. Generally, prostate cancer bone metastasis results in mixed but osteoblastic (more bone formation) dominant lesions, while breast cancer leads to osteolytic (more bone destruction) lesions.[7] Decreased mineralization and crystallinity have been reported in animal models of prostate cancer metastasis,[25,39,40] which is in agreement with the formation of less mineralized woven bones at the lesion. In the breast cancer metastasis model presented here, both properties increased at the metaphysis region in the tumor-bearing tibiae where the most severe lesions exist, possibly due to the tissue's compensatory response in cortex to the trabecular bone loss caused by osteolysis lesions. Therefore, mineralization and crystallinity in metastatic

bones can vary markedly with different primary tumors. These two properties should be examined cautiously when applied as spectral markers to estimate fracture risk in metastasis.

Typically, bone minerals contain ~5 to 8 wt.% carbonate, predominantly in the form of type B carbonate substitution in which a PO_4^{3-} is replaced by a CO_3^{2-}.[32,33] The concentration of carbonate varies with the tissue age, mineral crystallinity, and bone-remodeling rate,[12,13] and, thus provides important information regarding bone quality. The peak at ~1070 cm^{-1} in the Raman spectrum of bone is generally assigned to the carbonate $\nu 1$ mode. Although the neighboring bands from phosphate $\nu 3$ (1076 cm^{-1}) and lipid (1060 cm^{-1}) could potentially interfere with the precision in peak height and area calculation, the ratio of carbonate (at 1070 cm^{-1}) and phosphate $\nu 1$ (960 cm^{-1}) have been calibrated with various weight% of carbonated apatite and validated as an efficient measure for carbonation quantification in bone.[32] Therefore, the Raman spectral parameter carbonate/phosphate $\nu 1$ reflects the carbonation level and has been suggested to be predictive for osteoporotic fractures.[10] With aging, the carbonation level increases possibly due to the accumulation of bicarbonate ions produced by osteoclasts in the tissue.[25] This is a particularly attractive hypothesis here, since metastasis-bearing bone has extremely elevated osteoclast activity. Previous RS studies on metastatic bones from the prostate cancer model showed significantly elevated carbonation level than controls. In the current study, breast cancer bone metastasis also caused significant and consistent enhancement in carbonate substitution across the entire measurement region (2 cm). In addition, such enhancement is positively correlated with the size of bone metastatic lesions. These results suggest that Raman-derived carbonate substitution parameter, i.e., carbonate/phosphate $\nu 1$, can potentially be used as a unique spectral marker to evaluate bone quality alteration with tumor progression and may provide important information for the prediction of pathological fractures.

In summary, the present paper investigated the potential of RS in assessing pathological fracture risk. An RS spectral marker has been discovered, reflective of bone degeneration and metastatic lesion development. Although this *ex vivo* study exploited conventional RS, it paved the road to noninvasive assessment of metastatic bone using SORS or RT.

Acknowledgments

The authors would like to thank the following funding agencies for their support: K25 National Institute of Health grant K25CA149194-01 (X. B.); Vanderbilt Breast Spore P50CA098131 (X. B., J. A. S., and J. S. N.); VA Career Development Award (J. A. S.); Vanderbilt Center for Bone Biology Program Project P01CA40035 (X. B., J. A. S., D. S. P., and J. S. N.); and National Institutes of Health S10RR027631 (D.S.P.). This work was also supported in part by Career Development Award No. 1IK2 BX001634 from the United States (U.S.) Department of Veterans Affairs, Biomedical Laboratory Research and Development Program.

References

1. American Cancer Society, *Cancer Facts and Figures 2014*, American Cancer Society, Atlanta, Georgia (2014).
2. R. E. Coleman, "Metastatic bone disease: clinical features, pathophysiology and treatment strategies," *Cancer Treat. Rev.* **27**(3), 165–176 (2001).
3. R. E. Coleman, "Clinical features of metastatic bone disease and risk of skeletal morbidity," *Clin. Cancer Res.* **12**(20), 6243s–6249s (2006).
4. G. D. Roodman, "Mechanisms of bone metastasis," *N. Engl. J. Med.* **350**(16), 1655–1664 (2004).
5. I. J. Diel, E. F. Solomayer, and G. Bastert, "Treatment of metastatic bone disease in breast cancer: bisphosphonates," *Clin. Breast Cancer* **1**(1), 43–51 (2000).
6. N. Kohno, "Treatment of breast cancer with bone metastasis: bisphosphonate treatment—current and future," *Int. J. Clin. Oncol.* **13**(1), 18–23 (2008).
7. G. Mundy, "Metastasis to bone: causes, consequences and therapeutic opportunities," *Nature Rev.: Cancer* **2**(8), 584–593 (2002).
8. J. A. Hipp, A. E. Rosenberg, and W. C. Hayes, "Mechanical properties of trabecular bone within and adjacent to osseous metastases," *J. Bone Miner. Res.* **7**(10), 1165–1171 (1992).
9. T. S. Kaneko et al., "Mechanical properties, density and quantitative CT scan data of trabecular bone with and without metastases," *J. Biomech.* **37**(4), 523–530 (2004).
10. B. R. McCreadie et al., "Bone tissue compositional differences in women with and without osteoporotic fracture," *Bone* **39**(6), 1190–1195 (2006).
11. D. Bazin et al., "Diffraction techniques and vibrational spectroscopy opportunities to characterise bones," *Osteoporos. Int.* **20**(6), 1065–1075 (2009).
12. M. D. Morris and G. S. Mandair, "Raman assessment of bone quality," *Clin. Orthop. Relat. Res.* **469**(8), 2160–2169 (2011).
13. O. Akkus et al., "Aging of microstructural compartments in human compact bone," *J. Bone Miner. Res.* **18**(6), 1012–1019 (2003).
14. X. Bi et al., "Raman and mechanical properties correlate at whole bone-and-tissue levels in a genetic mouse model," *J. Biomech.* **44**(2), 297–303 (2011).
15. M. V. Schulmerich et al., "Transcutaneous Raman spectroscopy of murine bone in vivo," *Appl. Spectrosc.* **63**(3), 286–295 (2009).
16. N. A. Macleod and P. Matousek, "Deep noninvasive Raman spectroscopy of turbid media," *Appl. Spectrosc.* **62**(11), 291A–304A (2008).
17. P. Matousek et al., "Subsurface probing in diffusely scattering media using spatially offset Raman spectroscopy," *Appl. Spectrosc.* **59**(4), 393–400 (2005).
18. P. Matousek et al., "Noninvasive Raman spectroscopy of human tissue in vivo," *Appl. Spectrosc.* **60**(7), 758–763 (2006).
19. F. W. Esmonde-White et al., "Biomedical tissue phantoms with controlled geometric and optical properties for Raman spectroscopy and tomography," *Analyst* **136**(21), 4437–4446 (2011).
20. J. H. Demers et al., "Multichannel diffuse optical Raman tomography for bone characterization in vivo: a phantom study," *Biomed. Opt. Express* **3**(9), 2299–2305 (2012).
21. J. P. Campbell et al., "Models of bone metastasis," *J. Vis. Exp.* **67**, e4260 (2012).
22. J. J. Yin et al., "TGF-beta signaling blockade inhibits PTHrP secretion by breast cancer cells and bone metastases development," *J. Clin. Investig.* **103**(2), 197–206 (1999).
23. T. A. Guise et al., "Evidence for a causal role of parathyroid hormone-related protein in the pathogenesis of human breast cancer-mediated osteolysis," *J. Clin. Investig.* **98**(7), 1544–1549 (1996).
24. D. S. Perrien et al., "Inhibin A is an endocrine stimulator of bone mass and Sstrength," *Endocrinology* **148**(4), 1654–1665 (2007).
25. X. Bi et al., "Prostate cancer metastases alter bone mineral and matrix composition independent of effects on bone architecture in mice—a quantitative study using microCT and Raman spectroscopy," *Bone* **56**(2), 454–460 (2013).
26. C. A. Lieber and A. Mahadevan-Jansen, "Automated method for subtraction of fluorescence from biological Raman spectra," *Appl. Spectrosc.* **57**(11), 1363–1367 (2003).
27. R. E. Coleman, "Future directions in the treatment and prevention of bone metastases," *Am. J. Clin. Oncol.* **25**(6), S32–S38 (2002).
28. O. Akkus, F. Adar, and M. B. Schaffler, "Age-related changes in physicochemical properties of mineral crystals are related to impaired mechanical function of cortical bone," *Bone* **34**(3), 443–453 (2004).
29. M. Raghavan et al., "Age-specific profiles of tissue-level composition and mechanical properties in murine cortical bone," *Bone* **50**(4), 942–953 (2012).
30. N. P. Camacho et al., "The material basis for reduced mechanical properties in oim mice bones," *J. Bone Miner. Res.* **14**(2), 264–272 (1999).

31. S. Gamsjaeger et al., "Cortical bone composition and orientation as a function of animal and tissue age in mice by Raman spectroscopy," *Bone* **47**(2), 392–399 (2010).
32. A. Awonusi, M. D. Morris, and M. M. J. Tecklenburg, "Carbonate assignment and calibration in the Raman spectrum of apatite," *Calcif. Tissue Int.* **81**(1), 46–52 (2007).
33. G. Penel et al., "MicroRaman spectral study of the PO4 and CO3 vibrational modes in synthetic and biological apatites," *Calcif. Tissue Int.* **63**(6), 475–481 (1998).
34. J. S. Yerramshetty and O. Akkus, "The associations between mineral crystallinity and the mechanical properties of human cortical bone," *Bone* **42**(3), 476–482 (2008).
35. A. J. Makowski et al., "Polarization control of Raman spectroscopy optimizes the assessment of bone tissue," *J. Biomed. Opt.* **18**(5), 055005 (2013).
36. M. Kazanci et al., "Raman imaging of two orthogonal planes within cortical bone," *Bone* **41**(3), 456–461 (2007).
37. M. Kazanci et al., "Bone osteonal tissues by Raman spectral mapping: orientation-composition," *J. Struct. Biol.* **156**(3), 489–496 (2006).
38. M. Raghavan et al., "Quantitative polarized Raman spectroscopy in highly turbid bone tissue," *J. Biomed. Opt.* **15**(3), 037001 (2010).
39. K. A. Esmonde-White et al., "Raman spectroscopy of bone metastasis," *Proc. SPIE* **8207**, 82076P (2012).
40. X. Bi et al., "Characterization of bone quality in prostate cancer bone metastases using Raman spectroscopy," *Proc. SPIE* **7548**, 75484L (2010).

Hao Ding received his BS in physics from Nanjing University, China, and a PhD in biophysics from University of Michigan. He is currently a postdoctoral fellow in the Department of Nanomedicine and Biomedical Engineering, University of Texas Health Science Center Houston.

Jeffry S. Nyman, PhD, is an assistant professor of orthopaedic surgery and rehabilitation and biomedical engineering at Vanderbilt University. Prior to joining the Vanderbilt Center for Bone Biology, he was a postdoctoral fellow at the University of Texas at San Antonio, where he studied hard tissue mechanics. The ultimate goal of his research is to lower the number of bone fractures associated with osteoporosis, diabetes, cancer, genetic diseases, and aging.

Julie A. Sterling received her PhD in biomedical sciences from the Medical College of Ohio and completed postdoctoral training with Dr. Gregory Mundy at the University of Texas Health Science Center at San Antonio and Vanderbilt University. She is currently a research scientist at the Department of Veterans Affairs Tennessee Valley Healthcare System and an assistant professor in the Vanderbilt Center for Bone Biology. Her research focuses on studying signaling pathways that regulate skeletal metastases.

Daniel S. Perrien received his PhD from the University of Arkansas for Medical Sciences and worked at a biotechnology firm before joining Vanderbilt. He is currently a health research scientist at the Department of Veterans Affairs Tennessee Valley Healthcare System and an assistant professor in orthopaedic surgery and rehabilitation. His work focuses on understanding mechanisms that alter bone formation in a variety of conditions, including changes in mechanical loads, heterotopic ossification, and loss of gonadal function.

Anita Mahadevan-Jansen received her BS and MS degrees in physics from the University of Bombay, India, and MS and PhD degrees in biomedical engineering from the University of Texas at Austin. She joined the Vanderbilt engineering faculty in 1996. She is currently the Orrin H. Ingram professor of biomedical engineering at Vanderbilt University and holds a secondary appointment in the Department of Neurological Surgery.

Xiaohong Bi is an assistant professor of nanomedicine and biomedical engineering at the University of Texas Health Science Center at Houston, Texas. She received her BS in biochemistry from Nanjing University, China, and her MS and PhD in chemistry from Rutgers University, Newark, New Jersey. Her research focuses on the development of optical techniques for bone mineralization, pathogenesis characterization, and cancer theragnosis.